

Dalton Transactions

Accepted Manuscript



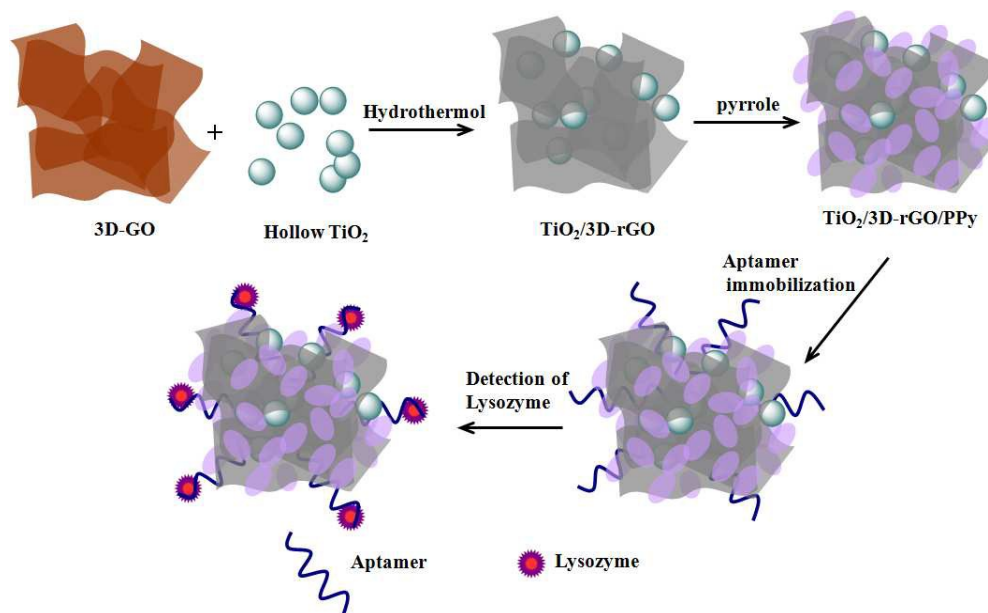
This is an *Accepted Manuscript*, which has been through the Royal Society of Chemistry peer review process and has been accepted for publication.

Accepted Manuscripts are published online shortly after acceptance, before technical editing, formatting and proof reading. Using this free service, authors can make their results available to the community, in citable form, before we publish the edited article. We will replace this *Accepted Manuscript* with the edited and formatted *Advance Article* as soon as it is available.

You can find more information about *Accepted Manuscripts* in the [Information for Authors](#).

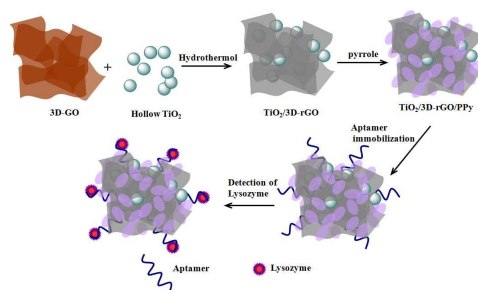
Please note that technical editing may introduce minor changes to the text and/or graphics, which may alter content. The journal's standard [Terms & Conditions](#) and the [Ethical guidelines](#) still apply. In no event shall the Royal Society of Chemistry be held responsible for any errors or omissions in this *Accepted Manuscript* or any consequences arising from the use of any information it contains.

Graphical Abstract



A sensitive aptasensor based on a nanocomposite of TiO₂/3D-rGO/PPy was developed for lysozyme detection. Using this strategy, a low limit of detection of 0.085 ng mL⁻¹ (5.5 pM) for detecting lysozyme was observed within the detection range of 0.1–50 ng·mL⁻¹ (0.007–3.5 nM). The aptasensor also presents high specificity for lysozyme, which is unaffected by the coexistence of other proteins. Such an aptasensor opens a rapid, selective, and sensitive route to lysozyme detection.

A table of contents entry



A sensitive aptasensor based on a nanocomposite of TiO₂/3D-rGO/PPy was developed for lysozyme detection

ARTICLE

An electrochemical aptasensor based on TiO₂/three-dimensional reduced graphene oxide/PPy nanocomposite for the sensitive detection of lysozyme

Cite this: DOI: 10.1039/x0xx00000x

Received 00th January 2012,
Accepted 00th January 2012

DOI: 10.1039/x0xx00000x

www.rsc.org/

Minghua Wang^{a,b}, Shuyong Zhai^b, Zihan Ye^b, Linghao He^b, Donglai Peng^b, Xiaozhong Feng^b, Yanqin Yang^{a,b}, Shaoming Fang^{a,b}, Hongzhong Zhang^{*a,b}, Zhihong Zhang^{*a,b}

A sensitive aptasensor based on a nanocomposite of hollow titanium dioxide nanoball, three-dimensional reduced graphene oxide, and polypyrrole (TiO₂/3D-rGO/PPy) was developed for lysozyme detection. Lysozyme aptamer was easily immobilized onto TiO₂/3D-rGO/PPy nanocomposite matrix by assembling the aptamer onto graphene through simple π -stacking interactions and electrostatic interaction between PPy molecular chains and aptamer strands. In the presence of lysozyme, the aptamer on the adsorbent layer caught the target on the electrode interface, which generates a barrier for electrons and inhibits electron transfer, subsequently resulting in decreased electrochemically differential pulse voltammetric signals of gold electrode modified with TiO₂/3D-rGO/PPy. Using this strategy, a low limit of detection of 0.085 ng mL⁻¹ (5.5 pM) for detecting lysozyme was observed within the detection range of 0.1–50 ng mL⁻¹ (0.007–3.5 nM). The aptasensor also presents high specificity for lysozyme, which is unaffected by the coexistence of other proteins. Such an aptasensor opens a rapid, selective, and sensitive route to lysozyme detection. This finding indicates that TiO₂/3D-rGO/PPy nanocomposite could be used as electrochemical biosensor for detecting proteins in the biomedical field.

Introduction

The detection and quantification of proteins play essential roles in fundamental research and clinical applications.¹ Lysozyme is a ubiquitous enzyme widely distributed in diverse organisms (e.g., bacteria, bacteriophages, fungi, plants, and animals) and is often termed as the “body’s own antibiotic.” Lysozyme, which has a primary sequence containing 129 amino acids, has a molecular weight of 14.4 kDa.^{2,3} Given the high affinity and specificity of aptamers to a wide range of target molecules (e.g., drugs, proteins, and other organic or inorganic molecules), aptamers as alternatives to antibodies become molecular recognition elements in biosensor application.⁴ Various analytical technologies exist for aptasensor, such as quartz crystal microbalance,^{5,6} surface plasma resonance,^{7,8} fluorescence,^{9,10} electrochemistry,^{11–13} and colorimetry.^{14,15} Given the

high sensitivity, simple instrumentation, portability, and inexpensiveness¹⁶ of the electrochemical method, it is attracting substantial attention in aptasensor development.

In recent years, a few electrochemical aptasensors for lysozyme recognition and detection have been developed. For instance, Peng et al. fabricated a label-free and sensitive faradic impedance spectroscopy aptasensor (FIS) based on target-induced aptamer displacement for lysozyme determination.¹⁷ The decrease in FIS signal is linear with increased concentration of lysozyme from 0.2 nM to 4.0 nM, with a limit of detection (LOD) of 0.07 nM. Rodríguez *et al.* have proposed an elegant label-free electrochemical aptasensor for lysozyme detection using an antilysozyme aptamer-modified carbon paste electrode.¹⁸ Chen et al. demonstrated a signal-off architecture for an electrochemical aptasensor to detect lysozyme at trace level, with the concentration of lysozyme within 7–30 nM and an LOD of 0.45 nM.¹⁹ The properties of the biosensor substantially depend on the adsorbent layer for biomolecule immobilization.

To improve the adsorbed amount of DNA or aptamer chains, polypyrrole (PPy) can be considered as a promising material with several characteristics, such as relative good conductivity, easy synthesis, and low cost. Studies have also been conducted on the biosensor applications of PPy. For instance, PPy has been directly electro-polymerized onto porous silicon substrate and used as

^aCollaborative Innovation Center of Environmental Pollution Control and Ecological Restoration

^bState Laboratory of Surface and Interface Science of Henan Province,

Zhengzhou University of Light Industry, No. 166, Science Avenue, Zhengzhou 450001, P. R. China.

Tel.: +86-37186609676

Fax: +86-37186609676

E-mail addresses: mainzh@163.com or zhz@zzuli.edu.cn

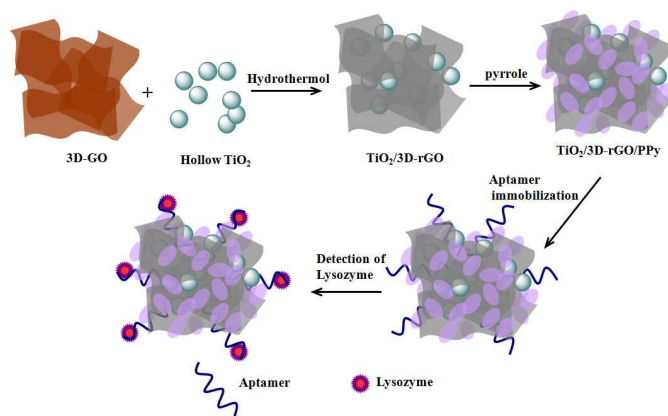
sensitive layer for DNA immobilization.²⁰ PPy-based adsorbents have been applied in the selective adsorption of bovine serum albumin and lysozyme in aqueous solutions at different pH values.²¹ Compared with nanomaterials, the electrochemical properties of PPy are relatively poor. Consequently, PPy is often modified with nanomaterials to improve their electrochemical performances and surface area. Moreover, the three-dimensional (3D) graphene network formation of sensitive layer could increase adsorption positions and is a beneficial immobilization platform for biomolecules. 3D reduced graphene oxide (rGO), hereafter denoted as 3D-rGO, with high surface-to-volume reaction and good in-plane conductivity have been used as matrices to immobilize redox probes and antibodies.²² Additionally, over the last few years titanium dioxide (TiO₂) has been used as a viable photocatalyst and is attracting considerable interest because of its excellent chemical and photochemical stability, high availability, low cost, and nontoxicity.²³ Recently, nanosized TiO₂ has been used to affix to biomacromolecules such as enzymes to achieve good biocompatibility and electron-transfer ability.^{24, 25}

Considering the synergistic effect among different types of nanomaterials and the combination of advantages of components, an electrochemical aptasensor based on a nanocomposite of TiO₂, 3D-rGO and PPy (TiO₂/3D-rGO/PPy) nanocomposite was fabricated through a one-step hydrothermal approach and used for lysozyme detection, as shown in Scheme 1. Compared with other electrochemical aptamer biosensors, the developed TiO₂/3D-rGO/PPy biosensor has three advantages for biomolecule immobilization, including i) large surface area, rich π -conjugation structure, and good in-plane conductivity caused by the presence of 3D-rGO, ii) porous structure of TiO₂ hollow nanoballs, and iii) imine groups in PPy molecular chains.

Results and discussion

Chemical components and crystal structure characterizations

FTIR and XRD were used to confirm the binding function between TiO₂, 3D-rGO, and PPy. Fig. 1a exhibits the FTIR spectra of



Scheme 1. Schematic of TiO₂/3D-rGO/PPy aptasensor for detecting lysozyme.

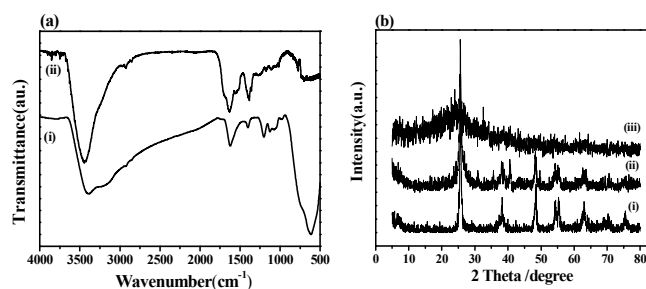


Fig. 1 (a) FTIR spectra of (i) TiO₂/3D-rGO and (ii) TiO₂/3D-rGO/PPy nanocomposites, and (b) XRD patterns of (i) TiO₂, (ii) TiO₂/3D-rGO, and (iii) TiO₂/3D-rGO/PPy nanocomposites.

TiO₂/3D-rGO and TiO₂/3D-rGO/PPy nanocomposites. The wide peaks at 400–600 cm⁻¹ is attributed to the stretching vibration of Ti–O–Ti bonds in crystalline TiO₂. (curve i). In the case of 3D-rGO/TiO₂/PPy (curve ii), the appearance of the strong absorption peak at 3450 cm⁻¹ suggests the presence of N–H stretching on pyrrole rings. The band at 1635 cm⁻¹ can be due to C=N stretching and N–H bending. The band at 1464 cm⁻¹ corresponds with =CH in-plane vibration, and the peak at 780 cm⁻¹ is due to =CH out-of-plane vibration.²⁶ The stretching vibration of C–N bonds shows a band at 1320 cm⁻¹, and the band at 1200 cm⁻¹ corresponds with C–C stretching. The band at 1040 cm⁻¹ is assigned to the in-plane deformation of C–H and N–H bonds of pyrrole ring. All these findings prove the presence of PPy in TiO₂/3D-rGO/PPy nanocomposite.

The phase structure and crystallinity of obtained samples were determined by XRD analysis. Fig. 1b presents the XRD patterns of TiO₂, TiO₂/3D-rGO and TiO₂/3D-rGO/PPy nanocomposites. The characteristic diffraction peaks of TiO₂ (curve i) and rGO/TiO₂ (curve ii) at 25.3°, 37.8°, 48.0°, 53.9°, 55.1°, 62.7°, 68.8°, 70.3°, and 75.0° can be indexed to (101), (004), (200), (105), (211), (204), (116), (220), and (215) crystal planes of anatase TiO₂ (JCPDS card no. 21-1272), respectively. As for TiO₂/3D-rGO/PPy nanocomposite, peaks with respect to anatase TiO₂ are lower than that with respect to TiO₂/3D-rGO or pure TiO₂ (curve iii). Thus, the polymerization of PPy is assumed to occur on TiO₂ surface and can suppress TiO₂ crystallite growth. Moreover, no diffraction peak is observed for graphene component (normally at ~25°) in TiO₂/3D-rGO and TiO₂/3D-rGO/PPy because of its low percentage and peak overlap with anatase phase at 25.3°.^{27, 28}

XPS were performed to investigate the chemical nature of TiO₂/3D-rGO and TiO₂/3D-rGO/PPy samples. C1s core-level spectra of TiO₂/3D-rGO nanocomposite (Fig. 2a) show the presence of four typical peaks of carbon bonds. The peak located at 284.72 eV is characteristic of graphitic carbon, and the bands at 285.65, 287.46, and 288.94 eV are assigned to C–O, C=O, and O–C=O bonds, respectively. The presence of O–C=O structures reveal that –OH groups on TiO₂ possibly react with –COOH groups on GO surface through esterification to form O=C–O–Ti bonds.²⁹ Ti 2p XPS data (Fig. 2b) exhibit two characteristic peaks at 459.08 and 464.79 eV, corresponding with Ti 2p_{3/2} and Ti 2p_{1/2} spin-orbit peaks of TiO₂.

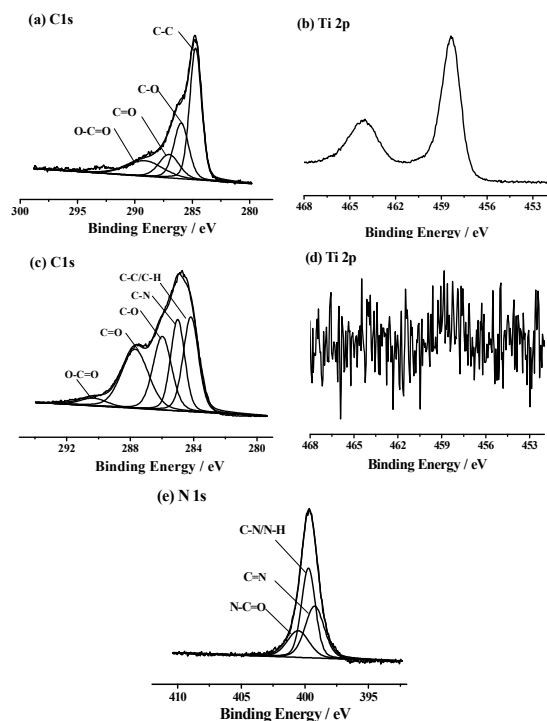


Fig. 2 C 1s (a) and Ti 2p (b) core-level XPS spectra of $\text{TiO}_2/3\text{D-rGO}$, and C 1s. (c) Ti 2p (d) and N 1s (e) core-level XPS spectra of $\text{TiO}_2/3\text{D-rGO/PPy}$ samples.

According to the XPS spectra of $\text{TiO}_2/3\text{D-rGO/PPy}$ nanocomposite (Figs. 2c–2e), binding energies of C1s, Ti2p, and N1s are around 284.81, 458.87, and 399.66 eV, respectively. Corresponding with $\text{TiO}_2/3\text{D-rGO}$ sample, the peak at 285.00 eV exhibits contributions from C–N bond observed in the pyrrole rings of conjugated PPy structure. Peaks at 284.17, 285.97, 287.69, and 290.31 eV are designated to C–C/C–H, C–O, C=O and O–C=O bonds, respectively.

N1s core-level XPS spectra of the sample (Fig. 2e) mainly consist of three components, which can be deconvoluted into C=N (~399.24 eV), C–N/N–H (~399.73 eV), and N–C=O (~400.53 eV) groups. Results indicate the presence of PPy in $\text{TiO}_2/3\text{D-rGO/PPy}$ nanocomposite could improve the binding affinity of DNA strands on the surface of the developed composite matrix. In aqueous solution, $-\text{NH}_2$ groups prefer to ionize to form the positive charged $-\text{NH}_3^+$, which could interact with the negative charged phosphates groups of aptamer strands.³⁰

However, only a very weak Ti 2p signal is observed (Fig. 2d). This signal could be due to TiO_2 nanoparticle entrapped by PPy, and XPS could not probe the chemical components of the interior of sample (around 6–8 nm), thereby leading to insignificant signal obtained.

Morphology properties and crystal structure of nanocomposites

Morphologies of 3D-rGO, TiO_2 , $\text{TiO}_2/3\text{D-rGO}$, and $\text{TiO}_2/3\text{D-rGO/PPy}$ nanocomposites were characterized by FESEM and TEM. 3D interpenetrating porous structures of graphene sheets and TiO_2 are clearly observed (Fig. S2).

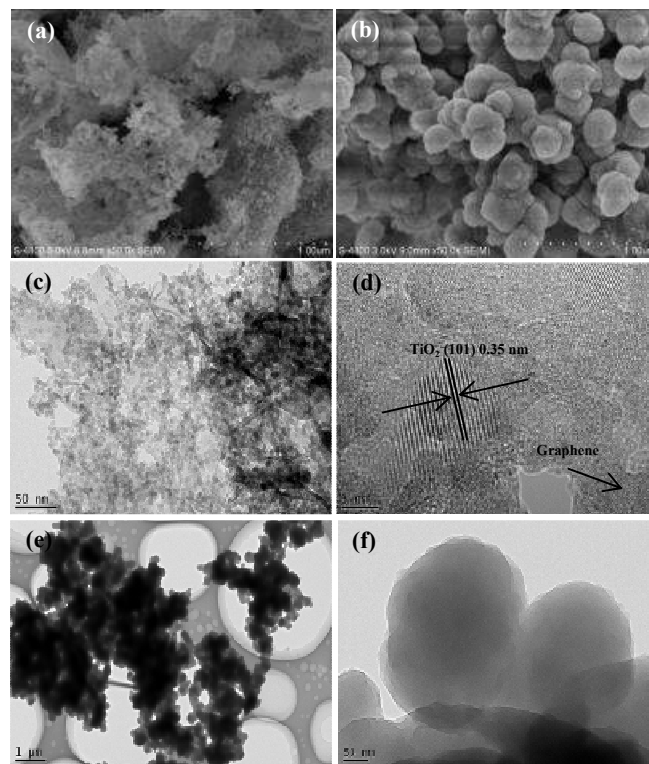


Fig. 3 SEM images of (a) $\text{TiO}_2/3\text{D-rGO}$ and (b) $\text{TiO}_2/3\text{D-rGO/PPy}$ nanocomposites. TEM images of (c and d) $\text{TiO}_2/3\text{D-rGO}$ and (e and f) TEM $\text{TiO}_2/3\text{D-rGO/PPy}$.

The morphology of $\text{TiO}_2/3\text{D-rGO}$ nanocomposites is shown in Fig. 3a. Hollow TiO_2 balls are broken into fragmented particles uniformly distributed onto folded 3D-rGO nanosheets. For the adsorbent layer, this morphology can facilitate biomolecule immobilization. After functionalization with PPy, the sample contains uniform spherical particles with a diameter of about 200 nm (Fig. 3b). TEM images of $\text{TiO}_2/3\text{D-rGO}$ nanocomposite (Fig. 3c) reveal the structure of rGO sheets with wrinkles, which are well anchored by spherical TiO_2 nanoparticles. Therefore, graphene sheets are good supports for TiO_2 nanoparticles. The spacings of the lattice fringes in $\text{TiO}_2/3\text{D-rGO}$ are ~0.35 nm (Fig. 3d), which could be assigned to crystalline planes of anatase TiO_2 (101). After polymerization of pyrrole monomer, particle diameters are around 200 nm, and the boundary of particles is very sharp (Figs. 3e–3f). Meanwhile, the boundary of graphene becomes ambiguous, which could be due to PPy covering the surface and interspaces of TiO_2 grains and to graphene.

Comparison of electrochemical properties of TiO_2 , $\text{TiO}_2/3\text{D-rGO}$, and $\text{TiO}_2/3\text{D-rGO/PPy}$ nanocomposites

To clarify the electrochemical properties of the resulting aptasensor, CV and DPV were used to monitor the fabrication of aptasensor for each step. Fig. 4a shows the CVs of different electrodes coated with TiO_2 , $\text{TiO}_2/3\text{D-rGO}$, and $\text{TiO}_2/3\text{D-rGO/PPy}$ nanocomposites in 0.1 M PBS (pH 7.4) containing 5 mM $\text{K}_3[\text{Fe}(\text{CN})_6]$ at a scan rate of 100 mV/s. Bare Au electrode, which has an obvious pair of redox peaks, is coated with TiO_2 nanoballs. Afterwards, current response

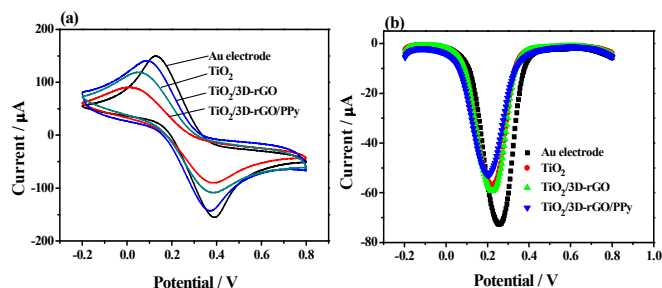


Fig. 4 (a) CV and (b) DPV curves of electrodes containing (i) TiO₂, (ii) TiO₂/3D-rGO, and (iii) TiO₂/3D-rGO/PPy nanocomposites in PBS containing 5 mM K₃[Fe(CN)₆].

obviously decreases because of the relatively low electron-transfer ability of TiO₂. Meanwhile, 3D-rGO could improve the electron-transfer ability of the composite electrode, leading to increased current response. By contrast, current response decreases when TiO₂/3D-rGO/PPy nanocomposite is coated onto the electrode, indicating that the presence of PPy with low conductivity decreases the electron-transfer rate. However, this finding demonstrates that the electrochemical properties of TiO₂/3D-rGO/PPy nanocomposite are higher than those of pristine PPy nanofilm, indicating that the presence of TiO₂ and 3D-rGO could enhance the electron-transfer activity of the composite electrode. Thus, the same trend of DPV measurements for different composite electrodes is obtained (Fig. 4b).

Lysozyme detection using the developed electrochemical biosensors

DPV measurements of samples at different stages and lysozyme detection are performed using [Fe(CN)₆]^{3-/4-} as redox maker. Figs. 5a–5c show DPV curves of the electrode at various stages for the detection of lysozyme ions based on three nanomaterials, i.e., TiO₂, TiO₂/3D-rGO, and TiO₂/3D-rGO/PPy. Bare Au electrode shows the largest current peak (I_p). After nanomaterials were composited with bare gold electrode, I_p decreases, indicating that nanomaterials are successfully immobilized onto Au electrode. The coverage of aptamer on the surface inhibits the access of electrons to the modified surface, leading to low electron-transfer efficiency of the system. After lysozyme detection, I_p continuously decreases, indicating that lysozyme further inhibits the access of electrons to the modified surface.

To evaluate the efficiency of lysozyme detection based on different biosensors, I_p values for each stage in lysozyme detection for the three samples are summarized in Fig. 5d. Differences in I_p values before and after the generation of a new layer adhesive (ΔI) could represent its relative amount. Among the three samples, lysozyme detection using the electrochemical biosensor based on TiO₂/3D-rGO/PPy nanocomposite lead to the highest variation of I_p , $\Delta I = 11.95 \mu\text{A}$. A low difference among ΔI values of 2.11 and 5.68 μA in case of TiO₂ and TiO₂/3D-rGO biosensors is observed after aptamer immobilization. Results show good affinity for lysozyme onto the developed electrochemical biosensor of TiO₂/3D-rGO/PPy

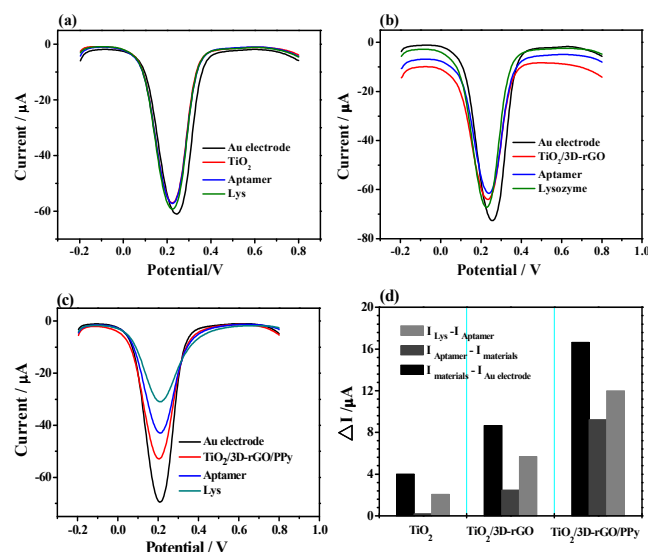


Fig. 5 DPV Curves of bare Au electrode vs. (a) TiO₂, (b) TiO₂/3D-rGO, and (c) TiO₂/3D-rGO/PPy nanocomposite-modified Au electrode, immobilized aptamer, and aptamer coordinated with lysozyme (0.5 ng mL⁻¹). (d) Variation in I_p for each stage in lysozyme detection was measured using developed biosensors, in which TiO₂, TiO₂/3D-rGO, and TiO₂/3D-rGO/PPy were used as sensitive layers.

nanocomposite. Relevant CV measurements are summarized in Fig. S3. Similar trends of electrochemical performance variations are observed among the three cases. Results indicate a synergistic interaction among the three components of TiO₂/3D-rGO/PPy nanocomposite toward the immobilization of aptamer molecules. As discussed elsewhere, DNA molecules can be adsorbed onto the surface of TiO₂ nanoparticles³¹ and onto graphene-related nanomaterials.³² The adsorption mechanism of DNA onto TiO₂ nanoparticles surface is not clearly understood. In the present work, even no substantial response change was observed after aptamer immobilized on the surface of TiO₂ spheres, there is a clear increase of ΔI after the addition of lysozyme. It indicates lysozyme was directly adsorbed onto the surface of TiO₂ spheres, but not bonded with aptamer. In other word, the presence of TiO₂ could enhance the adsorbed ability of lysozyme onto the nanomaterial. Moreover, the immobilization behavior of DNA onto graphene and its related materials is mainly due to multiple noncovalent interactions, including π - π stacking and hydrophobic interactions between DNA bases and graphitic domains of rGO.³³ All these phenomena can enhance the adsorption amount of DNA onto the composite electrode modified with TiO₂/3D-rGO/PPy nanocomposite.

Sensitivity of the developed biosensor based on TiO₂/3D-rGO/PPy nanocomposite

Analysis of samples at different stages and sensitive detection of the developed aptasensor toward lysozyme were performed by DPV measurements (Fig. 6). Current responses induced by lysozyme at different concentrations are evaluated (Fig. 6a). Peak current signals are found to decrease with increased lysozyme concentration. LOD

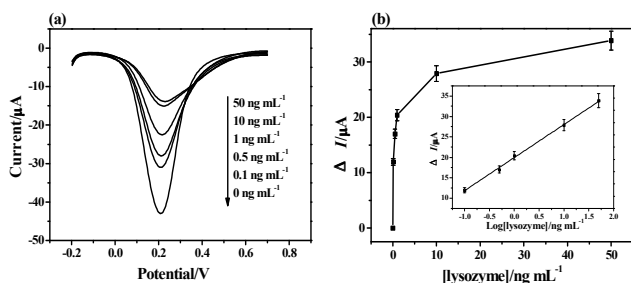


Fig. 6 (a) DPV curves of aptamer-immobilized $\text{TiO}_2/3\text{D-rGO/PPy}$ for lysozyme detection at different concentrations within 0.1–50 ng mL^{-1} . (b) Linear calibration curve for ΔI vs. $\log(C_{\text{lysozyme}} / \text{ng mL}^{-1})$, where C_{lysozyme} is lysozyme concentration.

Table 1 Comparison of sensitivities of different methods

Materials	Methods	Linear range	LOD	Ref.
MWCNTs/ionic liquids/chitosan	DPV	0.05–20 nM	6 pM	34
DNA duplex	square wave voltammetry (SWV)	7–30 nM	0.45 nM	19
$\text{Fe}_2\text{O}_3/\text{graphene}$	electrochemical impedance spectroscopy (EIS)	0.5–5 ng mL^{-1} (0.035–0.35 nM)	0.16 ng mL^{-1} (0.011 nM)	35
CdTe quantum dots	fluorescence	8.9–71.2 nM	4.3 nM	36
Gold nanoparticle	SWV	1–50 pg mL^{-1} (0.07–0.35 pM)	0.3 pg mL^{-1} (0.02 pM)	37
Chitosan–graphene oxide	EIS	0.25–1.5 $\mu\text{g mL}^{-1}$ (0.0175–0.105 μM)	0.38 $\mu\text{g mL}^{-1}$ (0.027 μM)	38

could be calculated using the parameters obtained from the regression curve.

The linear curve fits a regression equation of $\Delta I = 19.9597 + 8.1274 \log C_{\text{lysozyme}}$ within 0.1–50 ng mL^{-1} , with a correlation coefficient of 0.9977, as shown in Fig. 6b. LOD is estimated to be approximately 0.085 ng mL^{-1} (5.5 pM) at a signal-to-noise of 3, which is defined as lysozyme concentration corresponding with the signal and is equal to the zero signal minus three times the standard deviation. Compared with other works (Table 1), the developed aptasensor based on $\text{TiO}_2/3\text{D-rGO/PPy}$ for lysozyme detection exhibits high sensitivity.

Selectivity of aptasensor

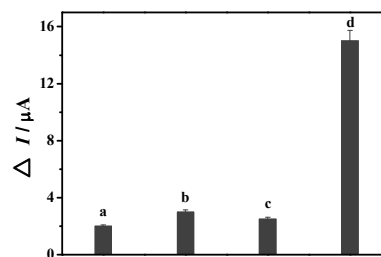


Fig. 7 Control experiments for aptamer- $\text{TiO}_2/3\text{D-rGO/PPy-Au}$ electrode after immersion in (a) 0.5 g mL^{-1} thrombin, (b) 0.5 g mL^{-1} BSA, (c) 0.5 g mL^{-1} BHb, and (d) 0.1 g mL^{-1} lysozyme.

An aptasensor must be both sensitive and specific to different analyte concentrations. Au electrode modified with $\text{TiO}_2/3\text{D-rGO/PPy}$ nanocomposite is immersed in 0.5 $\mu\text{g mL}^{-1}$ thrombin, 0.5 $\mu\text{g mL}^{-1}$ BSA, and 0.5 $\mu\text{g mL}^{-1}$ bovine hemoglobin (BHb) under the same experimental conditions and serves as the interference compound belonging to the same protein family as lysozyme. All proteins exist in the same environment as blood and have properties similar to those of lysozyme. Lysozyme is strongly associated with proteins having low isoelectric points (about 11, 7, 7.8 and 7.1 for lysozyme, thrombin, BSA, and BHb, respectively). Different DPV signals are shown in Fig. 7. After the incubation of thrombin with aptamer- $\text{TiO}_2/3\text{D-rGO/PPy-Au}$ electrode (column a), the value is calculated as 1.95 mA, similar to those of other cases (columns b and c). Interaction between lysozyme and modified Au electrode leads to a 15.20 mA increase in ΔI (column d), indicating that the aptasensor has high selectivity.

Storage stability and repeatability of aptasensor

The stability of a fabricated aptasensor is an important issue in its practical application in lysozyme detection. Therefore, the storage stability of the aptasensor was evaluated. Fig. 8 shows the time dependence of the relative signal change corresponding with the original signal of 0.1 $\mu\text{g mL}^{-1}$ lysozyme on the first of day measurement. Results indicate that in the presence of lysozyme, aptasensor response to 0.1 $\mu\text{g mL}^{-1}$ lysozyme is 90% of the original signal for one month (Fig. 8), indicating the good stability and life length of the aptasensor.

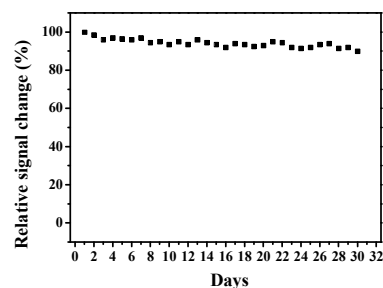


Fig. 8 Time dependence of relative signal change corresponding with the original signal of the proposed aptasensor at 0.1 $\mu\text{g mL}^{-1}$ lysozyme on the first day of measurement.

The usage repeatability of an aptasensor is highly significant in protein assay. Ten parallel-fabricated aptamer-TiO₂/3D-rGO/PPy-Au electrodes were used to detect 0.5 mg mL⁻¹ lysozyme. Bode plots of these electrodes before and after detection were recorded. An relative standard deviation (RSD) of 5.45 % for ΔI value is evaluated.

Application of aptasensor

To investigate the feasibility of applying this biosensor in the analysis of biological samples, lysozyme content in egg was examined. Lysozyme accounts for 3.5% of egg contents. Lysozyme in an egg white sample was diluted to 0.5 nM and then analyzed by DPV. The detected amount according to the standard curve is 0.513 nM, with a relative error of 2.60% (n = 3). In view of the activity of lysozyme in egg white, this result is still satisfactory.

Experimental

Materials

Graphite powder (99.95% purity), potassium permanganate, butyl titanate, and pyrrole monomer (99% purity) were analytical grade and purchased from Aldrich. Aptamer (5'-ATCAGGGCTAAAGAGTGCAGAGTTACTTAG-3') was purchased from Beijing SBS Genetech Co., Ltd. (China). Lysozyme was purchased from Beijing Solarbio Science & Technology Co., Ltd. (China). All other chemicals including anhydrous ethanol, hydrogen peroxide, hydrazine hydrate, and ammonium hydroxide were analytical grade and used as received.

Synthesis of TiO₂/3D-rGO nanocomposite

The preparation of 3D-GO and hollow TiO₂ nanoballs is detailed in Supporting Information. In a typical procedure, hollow TiO₂ nanoballs were dispersed in water by ultrasonication for 30 min, following by 3D-GO addition. Afterwards, ammonium hydroxide (3 mL) was added to the dispersion, which was stirred for 1 h. Hydrazine hydrate (2.5 mL) was then added, and the mixture was stirred for 2 h, placed in an autoclave, and dried at 180 °C for 24 h. Finally, the generated solid was filtered five times, dried at 120 °C for 24 h, and burned in a muffle furnace for 4 h, thereby producing TiO₂/3D-rGO nanocomposite.

Synthesis of TiO₂/3D-rGO/PPy nanocomposite

TiO₂/3D-rGO nanocomposite (10 mg) was dissolved in anhydrous ethanol (10 mL), pyrrole (100 mg) was added, and the solution was stirred in an ice-water bath for 30 min. Afterwards, ammonium persulfate (10 mL, 34 wt%) was slowly added to the solution. The solution became muddy 30 min later. Finally, the product was filtered using a vacuum suction filter device, washed with anhydrous ethanol and deionized water several times, and then dried at 40 °C for 8 h. The resulting solid was TiO₂/3D-rGO/PPy nanocomposite. After the analysis of the TGA data, the content of TiO₂, rGO, Ppy, and adsorbed water in the TiO₂/3D-rGO/PPy nanocomposite were about 7, 59, 25, and 9 wt.%, respectively (Fig. S5).

Preparation of phosphate buffer, aptamer, lysozyme, and electrolyte solutions

Aptamer and lysozyme solutions were prepared using phosphate buffer solution (PBS; pH 7.4) prepared by mixing 1/15 M Na₂HPO₄ and 1/15 M KH₂PO₄ in $\nu(\text{Na}_2\text{HPO}_4):\nu(\text{KH}_2\text{PO}_4) = (8:2)$. The electrolyte solution was immediately prepared before use by dissolving 1.65 g of K₃[Fe(CN)₆] and 2.11 g of K₄[Fe(CN)₆] in 1 L of PBS. All solutions were immediately prepared before the experiments and stored at -4 °C until use.

Aptamer immobilization onto TiO₂/3D-rGO/PPy and lysozyme detection

TiO₂/3D-rGO/PPy nanocomposite (0.5 mg) was added to anhydrous ethanol and thoroughly sonicated until a homogeneous suspension of TiO₂/3D-rGO/PPy was produced. Similarly, 0.5 mg/mL TiO₂ and 0.5 mg/mL TiO₂/3D-rGO homogeneous suspension was obtained. The suspension was stored under refrigeration at 4 °C.

Au electrodes (3 mm diameter, 7.065 mm²) were polished with 0.05 mm alumina slurries, ultrasonically washed in ultrapure water, and electrochemically cleaned through a series of oxidation and reduction cycling in 1.0 M H₂SO₄ from -0.4 V to 1.2 V (vs. Ag/AgCl). Aptamer immobilization was performed in a 200 nM aptamer solution of phosphate buffer for an immersion time of 8 h, and then the film was rinsed with PBS to remove excess aptamer molecules. Afterwards, the fabricated electrode was immersed in a lysozyme solution of phosphate buffer with different concentrations for 1 h. Changes in the electrochemical properties of the nanocomposite electrode were detected using cyclic voltammetry (CV) and differential pulse voltammetry (DPV).

Characterizations

Chemical components were analyzed by X-ray photoelectron spectroscopy (XPS) using a VG ESCALAB HP photoelectron spectrometer equipped with an analyzer and preparation chambers. X-ray diffraction (XRD) patterns were recorded on a Rigaku (Japan) D/Max r-A X-ray diffractometer with CuK α radiation. Fourier-transform infrared (FTIR) spectra were recorded on a Bruker TENSOR27 spectrometer (32 scans at 4 cm⁻¹ resolution). Surface morphology and structural analyses of samples were conducted with a JEOL JSM-6490LV field-emission scanning electron microscope (FE-SEM; JEOL Ltd., Tokyo, JAPAN) and a JEOL JEM-2100F transmission electron microscope (TEM; JEOL Ltd., Tokyo, Japan). A CHI 660D electrochemical analyzer (Shanghai Chenhua, China) connected with an Au electrode, an Ag/AgCl (saturated KCl) electrode, and platinum slides was used.

Electrochemical measurements

Electrochemical performances of the modified electrodes were evaluated by CV and DPV in 5 mM K₃[Fe(CN)₆]-K₄[Fe(CN)₆] (1:1) mixture as a redox probe in PBS (pH 7.4; containing 0.1 M KCl). CV was performed at a scan rate of 100 mV·s⁻¹ by potential scanning between -0.8 and 0.2 V. DPV was collected within the potential range of -0.2 V to 0.8 V with an amplitude of 50 mV and pulse width of 0.2 s. The electrochemical experiment data of the lysozyme detection were collected after 2 h at least until the system was stable.

Conclusions

A novel electrochemical aptasensor for lysozyme detection was developed based on TiO₂/3D-rGO/PPy nanocomposite. The electrochemical activity of PPy is found to be enhanced by the presence of 3D-rGO and hollow TiO₂ nanoballs, as proven by results of DPV and CV measurements. Electron transfer is also hindered by the blocking effect of aptamer immobilization, leading to decreased current response of Au electrode modified by TiO₂/3D-rGO/PPy composite. In the presence of lysozyme, aptamer on the adsorbent layer catches the target on the electrode interface, which makes a barrier for electrons and inhibits electron transfer, thereby resulting in decreased DPV signals of TiO₂/3D-rGO/PPy modified Au electrode. Furthermore, the proposed aptasensor has a very low LOD of 0.085 ng mL⁻¹ (5.5 pM). Given that DPV aptasensor possesses many advantages such as high sensitivity, selectivity, and stability, this approach could be adapted to aptamer-based detections of other proteins and small molecules.

Acknowledgements

This work is supported by the National Science Foundation of China (NSFC: Account No. 51173172) and Science and Technology Opening Cooperation Project of Henan Province (Account No. 132106000076).

References

- 1 D. Li, M. Kabir, D.J. Stuehr, D.L. Rousseau, and S-R. Yeh, *J. Am. Chem. Soc.* 2007, **129**, 6943.
- 2 A.K.H. Cheng, B. Ge, and H.Z. Yu, *Anal. Chem.* 2007, **79**, 5158.
- 3 L.D. Li, Z.B. Chen, H.T. Zhao, L. Guo, and X. Mu, *Sensor. Actuat. B* 2010, **149**, 110.
- 4 C. Deng, J. Chen, L. Nie, Z. Nie, and S. Yao, *Anal. Chem.* 2009, **81**, 9972.
- 5 Z.M. Dong, and G.C. Zhao, *Sensors* 2012, **12**, 7080.
- 6 B. Zheng, S. Cheng, W. Liu, M.H.W. Lam, and H. Liang, *Anal. Biochem.* 2013, **438**, 144.
- 7 C. Polonschii, S. David, S. Tombelli, M. Mascini, and M. Gheorghiu, *Talanta* 2010, **80**, 2157.
- 8 A. Vasilescu, S. Gaspar, I. Mihai, A. Tache, and S.C. Litescu, *Analyst* 2013, **138**, 3530.
- 9 B. Fu, J. Cao, W. Jiang, and L. Wang, *Biosens. Bioelectron.* 2013, **44**, 52.
- 10 K. Hu, J. Liu, J. Chen, Y. Huang, S. Zhao, J. Tian, and G. Zhang, *Biosens. Bioelectron.* 2013, **42**, 598.
- 11 Y. Wang, J. Feng, Z. Tan, and H. Wang, *Biosens. Bioelectron.* 2014, **60**, 218.
- 12 Y. Zheng, Y. Chai, Y. Yuan, and R. Yuan, *Anal. Chim. Acta* 2014, **834**, 45.
- 13 L. Bai, Y. Chai, X. Pu, and R. Yuan, *Nanoscale* 2014, **6**, 2902.
- 14 W. Jeon, S. Lee, D.H. Manjunatha, and C. Ban, *Anal. Biochem.* 2013, **439**, 11.
- 15 B.F. Ye, Y.J. Zhao, Y. Cheng, T.T. Li, Z.Y. Xie, and X.W. Zhao, *Nanoscale* 2012, **4**, 5998.
- 16 C. Deng, J. Chen, L. Nie, Z. Nie, and S. Yao, *Anal. Chem.* 2009, **81**, 9972.
- 17 Y. Peng, D. Zhang, Y. Li, H. Qi, Q. Gao, and C. Zhang, *Biosens. Bioelectron.* 2009, **25**, 94.
- 18 M.C. Rodriguez, and G.A. Rivas, *Talanta* 2009, **78**, 212.
- 19 Z. Chen, and J. Guo, *Electrochim. Acta* 2013, **111**, 916.
- 20 J. Jin, D. Zhang, E.C. Alocilja, and D.L. Grooms, *Ieee Sens. J.* 2008, **8**, 891.
- 21 X. Zhang, R. Bai, and Y.W. Tong, *Sep. Purif. Technol.* 2006, **52**, 161.
- 22 L. Li, W. Li, H. Yang, C. Ma, J. Yu, M. Yan, and X. Song, *Electrochim. Acta* 2014, **120**, 102.
- 23 C. Vila, and M. Rueping, *Green Chem.* 2013, **15**, 2056.
- 24 W. Tang, L. Li, and X. Zeng, *Talanta* 2015, **131**, 417.
- 25 K. Yan, R. Wang, and J. Zhang, *Biosens. Bioelectron.* 2014, **53**, 301.
- 26 Z. Zhang, S. Liu, M. Kang, G. Yang, Y. Li, F. Yan, L. He, X. Feng, P. Wang, and S. Ming, *Microchim. Acta* 2014, **181**, 1059.
- 27 P. Wang, Y. Tang, Z. Dong, Z. Chen, and T.T. Lim, *J. Mater. Chem. A* 2013, **1**, 4718.
- 28 W.L. Ong, M. Gao, and G.W. Ho, *Nanoscale* 2013, **5**, 11283.
- 29 Q. Xiang, J. Yu, and M. Jaroniec, *Nanoscale* 2011, **3**, 3670.
- 30 Z. Zhang, P. Liang, X. Zheng, D. Peng, F. Yan, R. Zhao, C.L. Feng, *Biomacromolecules* 2008, **9**, 1613.
- 31 T. Amano, T. Toyooka, and Y. Ibuki, *Sci. Total Environ.* 2010, **408**, 480.
- 32 Y. Xu, Q. Wu, Y. Sun, H. Bai, and G. Shi, *ACS Nano* 2010, **4**, 7358.
- 33 Z. Zhang, S. Liu, M. Kang, G. Yang, Y. Li, F. Yan, L. He, X. Feng, P. Wang, S. Fang, *Microchim. Acta* 2014, **181**, 1059.
- 34 A. Salim, S. Khezrian, R. Hallaj, and A. Vaziry, *Anal. Biochem.* 2014, **466**, 89.
- 35 M. Du, T. Yang, X. Guo, L. Zhong, and K. Jiao, *Talanta* 2013, **105**, 229.
- 36 S. Li, Z. Gao, and N. Shao, *Talanta* 2014, **129**, 86.
- 37 D. Xie, C. Li, L. Shanguan, H. Qi, D. Xue, Q. Gao, and C. Zhang, *Sensor. Actuat. B* 2014, **192**, 558.
- 38 A. Erdem, E. Eksin, and M. Muti, *Colloid. Surface. B* 2014, **115**, 205.